

Tests on High-Directivity Unconventional Biconical Type Antennas

Daniele Funaro

Dipartimento di Scienze Chimiche e Geologiche
Università di Modena e Reggio Emilia, Via Campi 103, 41125 Modena, Italy
daniele.funaro@unimore.it

Alessandro Chiolerio

Center for Bioinspired Soft Robotics
Istituto Italiano di Tecnologia, Via Morego 60, 16165 Genova, Italy
alessandro.chiolerio@iit.it

Abstract

Biconical-type antennas featuring high directivity have been designed, created, and tested in anechoic chamber. Results in the range between 1 and 5 GHz are presented in this article. In particular, two different configurations have been tested, with and without dielectric lenses, both involving rapid prototyping tools (3D printing) for the dielectric and the antenna support. A very high directivity is nowadays demanded by efficient and sustainable point-to-point communications or energy transfer protocols, to avoid releasing energy in neighboring areas and preserve data transfer security. As demonstrated here, special biconical type antennas featuring a 3D printed polylactic acid (PLA) dielectric lens can achieve a good directivity, with a corresponding emission lobe centered around 8.4 degrees, featuring a FWHM of 6.4 degrees. Dielectric lens-free antennas, featuring an unconventional shape, can also achieve a good directivity, with a corresponding emission lobe centered around 10.0 degrees, featuring a FWHM of 14.2 degrees. The preliminary results shown here explore some of the aspects of the vast configuration space (which include fabrication techniques, dielectric materials, conductive supports, etc.) and open the route for further optimization studies. The aim would be to adjust the various degrees of freedom in order to achieve what can be defined as “infinite” directivity.

Keywords: Biconical antenna; directive antenna; point-to-point transmission; wireless power transmission; 3D printing

1 Introduction

Highly directive antennas are an important tool in all applications where point-to-point communications need to be established. There are several reasons to justify their development, as for example to guarantee secure transmissions, to reduce the impact of electromagnetic fields on neighbouring areas or the interference between spatially distributed components, to increase the sustainability and therefore damp transmission losses in particular when a high power is radiated [1], [2]. There are currently two categories of commercial directive radio antennas [3]: on the one hand we find the traditional ones, including helix, log-periodic array, aperture horn, reflectors and patch antennas. On the other hand there are smart antennas, which have become known as “beam-forming” [4], consisting of an array of elements that can offer adaptive transmission. Optical means are also used to convey directional channels [5]. A recent use of dielectric lenses to correct the direction of the signal emitted is reported in [6]. Depending on the specific application, shapes, sizes and designs can be quite different. The polar signal pattern from a directional antenna typically consists of an elliptic principal lobe, usually surrounded by smaller side lobes. For a survey on radiation patterns and an application on wireless networks we mention for instance: [7], [8].

Biconical antennas have been used ever since in the transmission range between 30 and 200 MHz and their theory is known since the 1950s [9]. Extensions up to 1 GHz [10] and Ultra Wide Band applications (UWB) [11], have been recently implemented. Biconical antennas have been adopted in UWB Direction of Arrival (DoA) applications [12]. Asymmetric designs have also shown to provide beam shaping capabilities [13]. In space applications biconical antennas are also used (see, e.g., [14]), particularly for the low or medium gain segments, as reported for example in [15], where the directivity achieved by a corrugated design shows a Full Width at Half Maximum (FWHM) of about 50° . In this last case, the finality was to achieve a broad beam, which is exactly the opposite of what we would like to get here.

The results reported in the present paper come from the practical realization of the device proposed and designed in [16], where numerical simulations were also presented. The main peculiarity of this typology of antenna is that the signal departing from the emitter is composed by successive annular regions, traveling from the coaxial cable (TEM-mode) and emerging always preserving the same topology. A theory that predicts the existence of “solitary” waves that travel in free-space along straight patterns without dissipation, has been developed [17], [18]. This included the case in which the Poynting vectors are all parallel. Such an “infinite” directivity may be not achievable in practice. Nevertheless, starting from the preliminary test here reported, it is certainly possible to design more evolved prototypes that reproduce at their best such an extreme behavior.

Acknowledgements For their kind assistance, we are indebted with Prof E. Bassoli (3D printing of the versions C and D) and Prof. F. Leali (prepa-

ration of the aluminium reflector), Dipartimento di Ingegneria Enzo Ferrari, Università degli Studi di Modena e Reggio Emilia; Prof F. Auricchio (3D printing of the dielectric lenses), 3D@UniPV, Department of Civil Engineering and Architecture, Università degli Studi di Pavia; Prof. L. Ferraris, Dipartimento di Energia, Politecnico di Torino. Special thanks for the valuable support in the measurements process go to Dr. F. Franchini, Laboratorio di Compatibilità Elettromagnetica, Politecnico di Torino, located in Alessandria.

2 Biconical antennas with 3D printed dielectric

The antenna device is made of two conductive cones, having an angle of $\pi/2$ at the vertex, separated by a little gap. These conductors are supplied by an RF signal via a coaxial cable passing through one of the cones. The assembly is embedded in a volume occupied by a linear homogeneous medium, featuring a relative permittivity coefficient $\epsilon_r > 1$, whereas the magnetic permeability coefficient is μ_0 . The shape of the dielectric is designed in order to fulfill specific refraction properties as explained in [16]. A final conical metal reflector is added to the transmitting device, so obtaining the complete antenna as shown in Fig. 1.

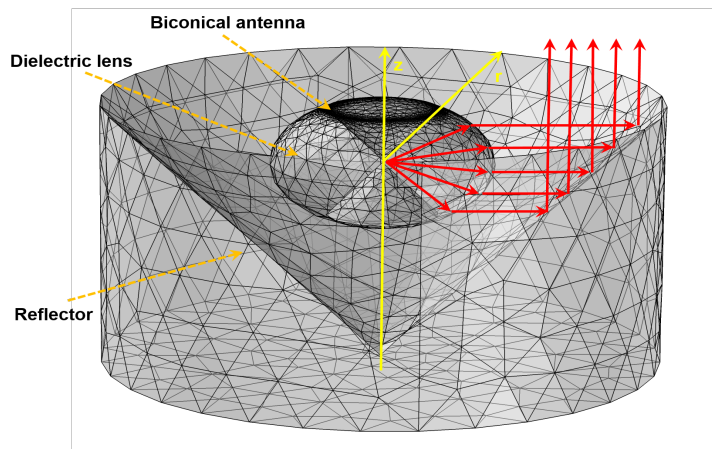


Figure 1: Scheme showing a rendering of the biconical antenna equipped with dielectric lens and reflector, as described in the manuscript. Here the emission axis is vertical.

The dream is to get an emitted signal with perfectly parallel rays, corresponding to infinite directivity. We will call *emission axis* (z) the straight-line naturally associated with the axis of both the cones and the reflector (Fig. 6). The electromagnetic wave, during its transition from inside the coax to the free

space, does not break the lines of force of the magnetic field. These remain closed curves encircling the emission axis. In this way, at all the steps of the transition, the whole signal maintains a cylindrical symmetry. Thus, the fields are zero near the emission axis and are polarized by following a kind of a circular fashion (Fig. 6, right).

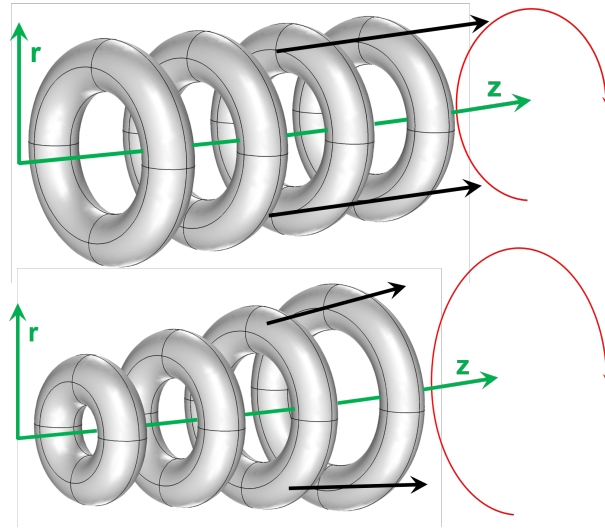


Figure 2: Behavior of a sinusoidal signal emerging from the antenna: perfect directivity (top), good directivity (bottom). Here the emission axis is horizontal.

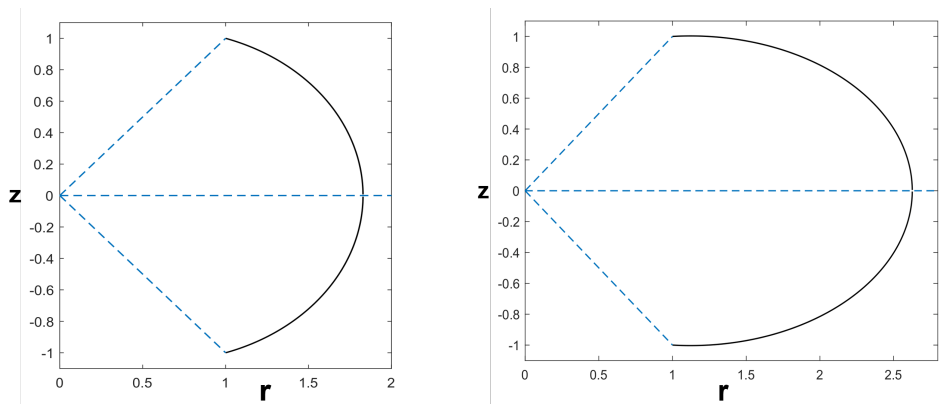


Figure 3: Profile of the dielectric lenses: Type A (left), Type B (right). The unit of measure of the distances is normalized. The vertical axis is parallel to the emission one, the horizontal axis indicates the radius of the device.

The shape of the emitted wave, modulated by sinusoidal frequency, is expected to look at its best as a sequence of equal toroidal regions (see Fig. 2, top), progressing at the speed of light. Nevertheless, this would be the ideal behavior. Indeed, in practical experiments, slightly diverging signals are obtained, as for instance in Fig. 2, bottom. We believe however that there is quite enough room to ameliorate these performances (see the discussion in the concluding section 6).

The dielectric lens-equipped antennas that have been tested, feature a core made by an ensemble of two copper cones and the whole structure embedded in a dielectric, namely polylactic acid (PLA), shaped by a 3D printing process by means of a fused deposition modelling (FDM) machine. We recall that the electric relative permittivity coefficient for PLA is about $\epsilon_r \approx 3.5$ [19]. Each dielectric is composed of two symmetric parts glued together, with a glue having a similar permittivity constant. On the other hand, the 3D printing of the entire structure would have been rather complicated.

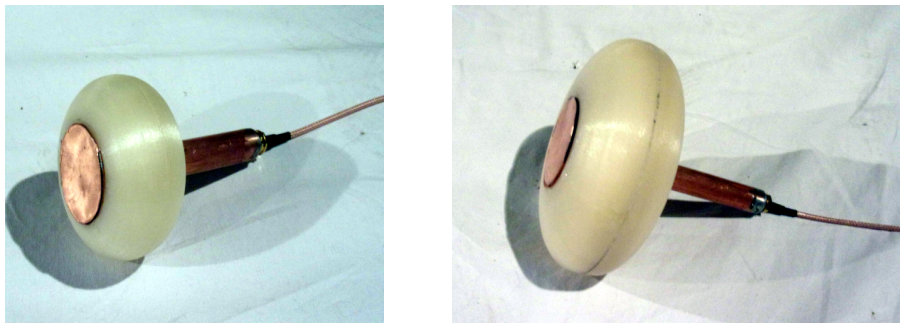


Figure 4: Biconic components supplied with their 3D printed dielectric: Type A (left), Type B (right).

The antenna of Type A features two copper cones of base 3 cm, height 1.5 cm. The dielectric part has a width of approximately 5.4 cm and height of 3 cm. Its shape has been chosen as suggested in [16], section 6, by a proper matching of the value of the relative permittivity, chosen to be $\epsilon_r = 4$ (thus a bit larger than the coefficient corresponding to PLA). The dielectric profile can be seen in Fig. 3 (left), and the final realization in Fig. 4 (left)

Type B features two copper cones having base 4 cm, height 2 cm. The dielectric lens has a width of approximately 10.4 cm and height of 4 cm. This time the profile has been chosen to a corresponding value of $\epsilon_r = 1.8$ (approximately a half of that of PLA). The dielectric profile can be seen in Fig. 3 (right), and the final realization in Fig. 4 (right). Even though the permittivity coefficients of both antenna prototypes do not match with those theoretically recommended, the choices are justified by the willing to test two rather different conditions. Since the 3D printing process for the dielectrics is quite time consuming, a very limited number of prototypes at this preliminary stage was produced.

3 Tests in anechoic chamber

A conic reflector (see Figs. 1, 5, 6) is used to convey the radiated waves towards the receiver. It features a 32 cm opening diameter, a vertex angle equal to $\pi/2$, and is manufactured using a lathe from a single piece of aluminium. Each antenna is centered and hosted inside the reflector, and finally supplied from the rear side via a SMA connector and cable.



Figure 5: Layout of the measurement area. Detail showing the aluminum reflector (top), hosting the biconical antenna surrounded by 3D printed dielectric. Overview of the anechoic chamber (bottom), where the log-periodic receiver can be glimpsed.

The measurements have been performed in an anechoic chamber equipped with a rotating table, using the following instrumentation: the tracking generator of a Rohde & Schwarz ESBI receiver with an output of 1 mW, a log-periodic

Rohde & Schwarz HL562 (in the frequency range between 500 MHz and 3 GHz), an Amplifier Research 30S1G3 stage supplying 30 W (in the frequency range between 1 GHz and 5 GHz), coupled with a horn antenna Rohde & Schwarz HF906. The height of the center of the device from the ground is 1 meter and the distance from the receiver is about 4 meters.

The entire biconical antenna is rotated horizontally about the vertex of the reflecting cone as shown in Fig. 6 (left). The angles range between 0° (emission axis pointing towards the receiver) up to 50° at steps of about 2° . For symmetry reasons, the tests are independent of the rotation sense, so that only one side was exploited. Figure 6 (right) gives an idea of the polarization of the electric field on the plane of observation.

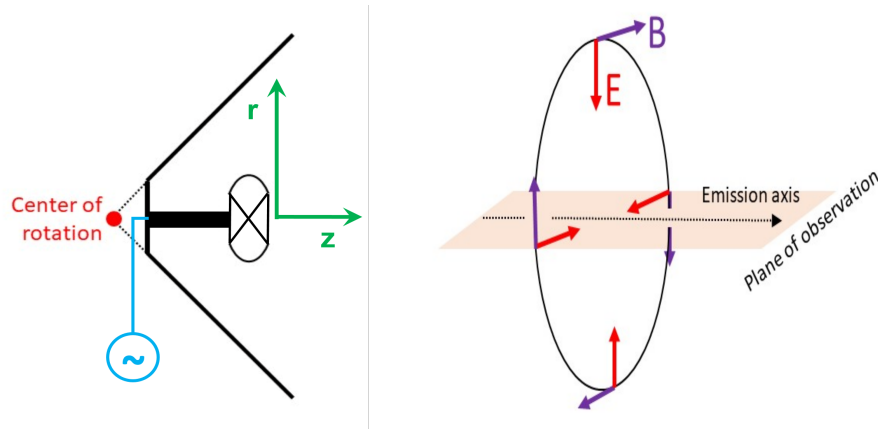


Figure 6: Fulcrum of rotation of the antenna (left), as seen from above, depicted with circuitual connection to the waveform generator and polar axes. The expected electric signal, measured on the horizontal plane containing the emission axis, is schematically displayed on the right. Note that the electric field is radial and the magnetic field rotates around the emission axis, which is parallel to the Poynting's vectors. Both fields vanish at the center of the circle.

Figure 7 shows the 2-dimensional contour plots of the measured received power, with angles from 0° to 45° , and frequencies ranging between 1 GHz and 3 GHz. The unity of measure of the instruments is given in Decibels per mW (dBm). As the scale is logarithmic with argument less than 1, the greatest emission strengths are those close to zero.

We are not aware of the impedance properties of the transmitting antennas, therefore we are unable to judge the efficiency of our devices. We believe that this is irrelevant at this stage, since here the primary concern is the direction of propagation of the signal. We have relatively good directivity when, for a given frequency, the patterns tend to be concentrated towards the small angles. For example, both antennas show scarce directivity below 1.5 GHz or above 2.5 GHz, while the intermediate frequency range looks much better. For frequencies

above 2.5 GHz a secondary lobe appears. We will provide more explanations of these results in the concluding section 6.

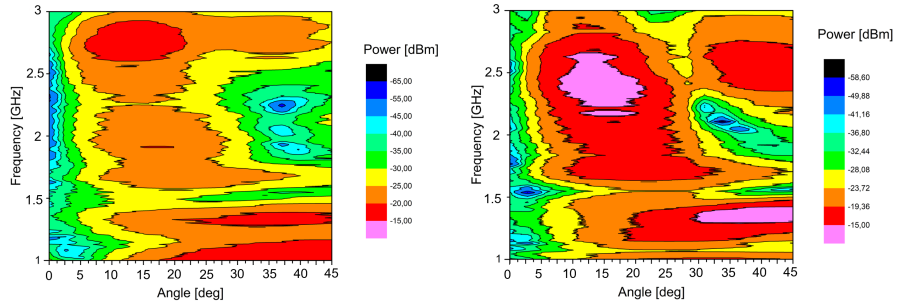


Figure 7: 2D plots of the antenna emission power in dBm, recorded with a log-periodic antenna: Type A (left), Type B (right). The frequency ranges from 1 GHz up to 3 GHz.

A more practical visualization is represented by the polar charts of Fig. 8. Here, we switched from dBm to the power expressed in mW using the conversion formula: $P = 10^{\{\text{dBm}/10^{-3}\}}$.

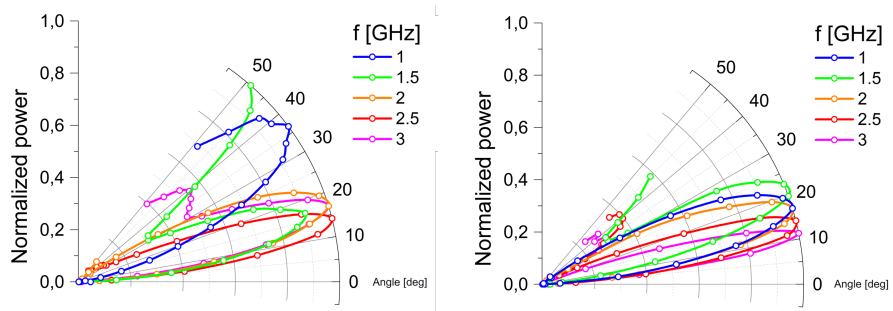


Figure 8: Polar diagrams of the normalized emission powers at selected frequencies 1, 1.5, 2, 2.5 and 3 GHz, recorded with the log-periodic receiver: Type A (left), Type B (right).

The results relative to the antenna of Type B show a more robust diagram of the emission pattern, where the principal lobes are comprised between 10° and 20° . Antenna of Type A shows the principal lobes distributed over a broader range, comprised between 10° and 50° . In addition, there are secondary lobes, showing up at frequencies above 1.5 GHz. These last are comprised in the

range between 30° and 50° . The optimal directivity was found for a frequency of about 2.3 GHz (antenna of Type A), with a lobe centered around 14° featuring a FWHM of 16.1° . Regarding the antenna of Type B, we get the best results when the frequency is about 1.69 GHz and the lobe attains its maximum around 19.6° , with a FWHM of 20.7° .

Theoretically, the adoption of a dielectric shape where the value $\epsilon_r > 3.5$ (we recall that 3.5 is the relative permittivity of PLA) is overestimated as in Fig. 3 (left), tends to spread the signal. Conversely, when ϵ_r is less than the suggested value 3.5, as in Fig. 3 (right), the signal tends to be over focussed, with the consequence that the rays may cross each other before reaching the reflector, resulting again in a spread of the emission. The right balance would follow from testing with many different shapes. This is however not an option in this preliminary analysis.

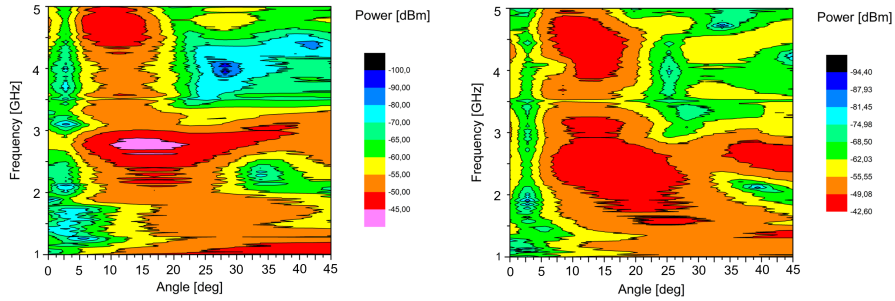


Figure 9: 2D plots of the antenna emission power in dBm, recorded with a horn antenna: Type A (left), Type B (right). The frequency ranges from 1 GHz up to 5 GHz.

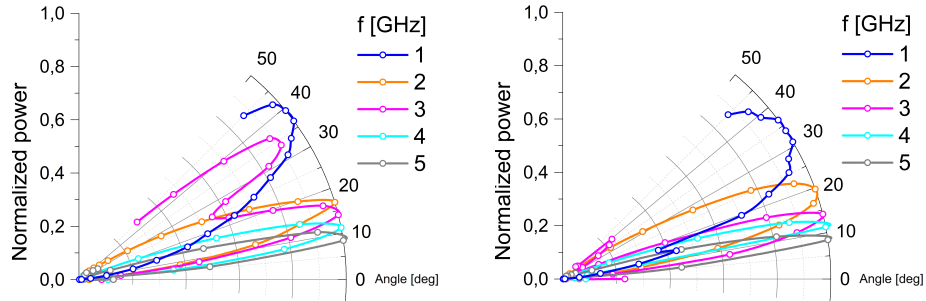


Figure 10: Polar diagrams of the normalized emission powers at selected frequencies 1, 2, 3, 4 and 5 GHz, recorded with the horn receiver: Type A (left), Type B (right).

Further data are available. These were recorded with a horn type antenna with an extended frequency ranging between 1 GHz and 5 GHz. Figure 9 shows the 2-dimensional contour plots of the emission power, measured for angles between 0° and 45° . Both antennas display a broad emission below 3.5 GHz, while in the higher frequency range the directivity looks extremely good.

The same results are displayed in the polar plane in Fig. 10, for some selected frequencies. These measurements confirm that the antenna of Type B provides better emission patterns, having in some cases the principal lobe distributed around 10° . Antenna of Type A shows principal lobes distributed over a broader range, comprised between 10° and 40° . A prominent secondary lobe appears for a frequency of 3.5 GHz, and is comprised in the range between 30° and 40° .

The optimal directivity for the antenna of Type A was found for a frequency of about 4 GHz. The corresponding lobe is centered around 8.4° , featuring a FWHM of 6.4° . Concerning the Type B antenna, the best performances are obtained for a frequency of about 3.66 GHz. The corresponding lobe is centered around 11.3° , featuring a FWHM of 9.9° .

A first explanation of the better performances at higher frequencies is that both the emitting devices are relatively small. The qualitative difference of the outcomes of figures 8 and 10 in the range of frequencies at the intersection (i.e.: 1 GHz to 3 GHz) can be justified by the type of antenna used as a receiver. In particular, the log-periodic antenna is much bulkier than the horn antenna. This affects experiments, since, theoretically, the received should be placed at infinite distance in order to probe high directivity emission patterns. More insight on these issues will be given in section 6.

4 Bare biconical antennas

Another set of biconical antennas was tested, using open air instead of the dielectric lens. The copper cones were replaced by two conductors having a complicated shape, so skipping the construction of the dielectric medium. 3D printed antennas were fabricated using insulating materials (antenna of Type C, made of PLA, with a base of 9 cm diameter and a height of 5.2 cm, see Fig. 11), or conductive materials (antenna of Type D, made of carbon black-compounded PLA, with a base of 9 cm diameter and a height of 4.5 cm, see Fig. 12), both ultimately coated using a conductive silver enamel, cured with hot air (90 degrees centigrade for 15 min).

The shapes of these devices were obtained through heuristic arguments, with the help some theoretical considerations that we do not report here. In order to be able to reproduce our experiments we provide the explicit expression of the radius r as a function of z , describing the curved profiles of the two devices. For $0 \leq z \leq \ell$, we have:

$$r(z) = \ell \left[\frac{6}{5} - \left(1 - \left(\frac{z}{\ell} \right)^\gamma \right)^{1/\gamma} \right] \quad r(z) = \ell \left[1 - \left(\frac{z}{\ell} \left(2 - \frac{z}{\ell} \right) \right)^{1/4} \right]$$

where ℓ is a scaling parameter and $\gamma = 1.9$.



Figure 11: Type C bare biconical antenna.



Figure 12: Type D bare biconical antenna.

Measurements have been done in the same anechoic chamber of the tests of the previous section using the log-periodic receiver and a frequency range between 1.5 GHz and 3 GHz. Figure 13 shows the 2-dimensional contour plots of the emission pattern measured by varying the angle from 0° to 80° , whereas Figure 14 shows the polar curves for some selected frequencies. Both types of transmitting antennas show a primary and secondary lobe emission between 2 GHz and 3 GHz, and an increasingly higher directivity at the higher frequencies. The antenna of Type C features a slightly better directivity and works well at lower frequencies, in comparison to the device of Type D. The optimal directivity was found for the frequency of 3 GHz for both types of antennas, with a lobe centered around 10° featuring a FWHM of 14.2° (Type C) and a lobe centered around 18° featuring a FWHM of 26.3° (Type D). The outcome is interesting, though still a bit far from optimality. Due to the lack of the dielectric lens correction, the wave grows with distance from the source, following a conical pattern.

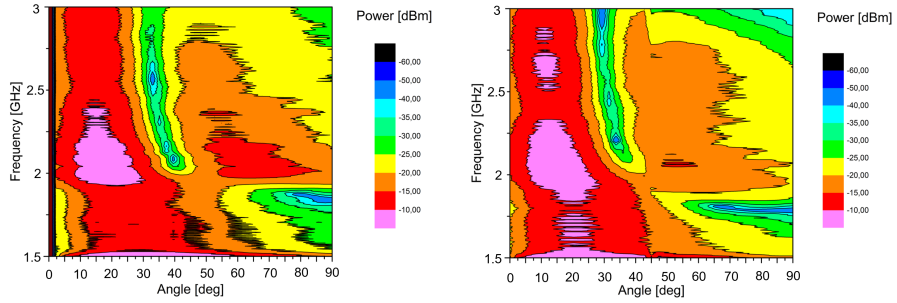


Figure 13: 2D plots of bare biconical antenna emission power in dBm, recorded with a log-periodic receiver: Type C (left), Type D (right). The frequency ranges from 1.5 GHz up to 3 GHz.

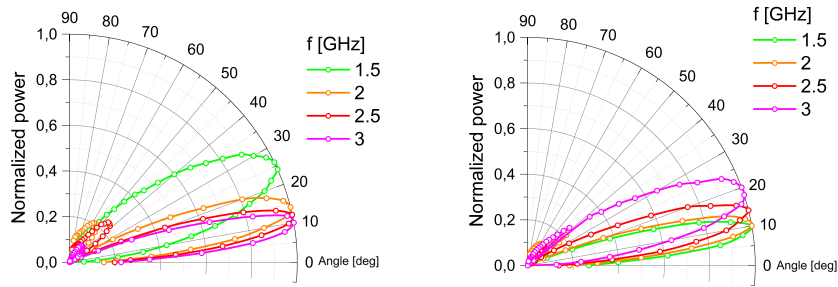


Figure 14: Polar diagrams of the normalized emission powers at selected frequencies of 1.5, 2, 2.5, and 3 GHz, recorded with the log-periodic receiver: Type C (left), Type D (right).

5 Theoretical justifications

The signals produced by the new types of antennas here presented are well described in cylindrical coordinates (r, ϕ, z) by the expression:

$$\mathbf{E} = (cf(r) \sin \omega(ct - z), 0, 0) \quad \mathbf{B} = (0, f(r) \sin \omega(ct - z), 0) \quad (1)$$

where c is the speed of light, \mathbf{E} and \mathbf{B} are the electric and magnetic fields respectively, and the function f is (almost) arbitrary. In particular, we can assign f in such a way it is globally continuous and zero outside a prescribed domain. Like in Fig. 2 (top), this solitary wave shifts at the speed of light along the emission axis (the z -axis in this case).

The wave described in (1) is only achievable in the case of infinite directivity. More likely, we have the conical type configuration of Fig. 2 (bottom). This can be described in spherical coordinates (r, θ, ϕ) by the following exact expression:

$$\mathbf{E} = \left(0, \frac{cf(\theta)}{r} \sin \omega(ct - r), 0\right) \quad \mathbf{B} = \left(0, 0, \frac{f(\theta)}{r} \sin \omega(ct - r)\right) \quad (2)$$

Here f could be allowed to be only different from zero in the circular annulus determined by $0 < \theta_{\min} < \theta_{\max} < \pi/2$. When θ_{\min} and θ_{\max} are small, we get a conical wave with a very reduced aperture.

We remark that very few of the above examples are included in the solutions space of Maxwell's equation in vacuum. Indeed, note that in general we have $\text{div}\mathbf{E} \neq 0$. For example, in (1) we can only have $\text{div}\mathbf{E} = 0$ when $f(r) = 1/r$. This last situation is compatible with a wave traveling in a coaxial cable in conditions of perfect conductivity. It is however necessary to drop the equation $\text{div}\mathbf{E} = 0$ if we want to simulate a similar behavior in free space. This a consequence of the vanishing boundary conditions to be imposed to the transverse electric field along the transition zone between the wave itself and the open space (i.e. outside the cylinder of Fig. 2 (top) or the cone of Fig. 2 (bottom)).

A quick check of these statements can be done in the case of a scalar wave equation in Cartesian coordinates. We look for a solution of the type $u(x, y, z, t) = f(x, y)g(ct \pm z)$, which is traveling along the z -axis. Here g is arbitrary and modulates the signal in the direction of propagation. We have:

$$\begin{aligned} \square u &= \frac{\partial^2 u}{\partial t^2} - c^2 \Delta u = \left(\frac{\partial^2 u}{\partial t^2} - c^2 \frac{\partial^2 u}{\partial z^2} \right) - c^2 \left(\frac{\partial^2 u}{\partial x^2} + \frac{\partial^2 u}{\partial y^2} \right) \\ &= -c^2 g \left(\frac{\partial^2 f}{\partial x^2} + \frac{\partial^2 f}{\partial y^2} \right) = 0 \end{aligned} \quad (3)$$

Therefore f turns out to be harmonic as a function of the variables x and y . Since f is required to vanish outside a bounded 2-D domain, then the only possibility is that $f \equiv 0$ (in fact, we have an elliptic problem with zero right-hand side and zero boundary conditions).

Note also that the equation $\square\mathbf{E} = 0$ is obtained under the assumption that $\text{div}\mathbf{E} = 0$. Indeed, we have:

$$\frac{\partial^2 \mathbf{E}}{\partial t^2} = c^2 \frac{\partial}{\partial t} \text{curl}\mathbf{B} = -c^2 \text{curl}(\text{curl}\mathbf{E}) = c^2 [\Delta\mathbf{E} - \nabla(\text{div}\mathbf{E})] = c^2 \Delta\mathbf{E} \quad (4)$$

Let us observe instead that it is always possible to arrange the distribution of the fields in such a way that $\text{div}\mathbf{B} = 0$. We just saw above that the solutions of the wave equation are very few. Hence, a spectrum of possible solutions is brought by admitting the possibility that $\text{div}\mathbf{E} \neq 0$ in suitable regions of space. As a final remark, we may observe that the set of Maxwell's equations in vacuum amounts to eight equations (two vector equations plus two scalar ones) with six unknowns (the components of the electric and magnetic fields), so that an incompatibility is expected. The possibility that $\text{div}\mathbf{E} \neq 0$ may

sound unphysical, since there is not presence of charges in vacuum. By the way is very useful from the technical viewpoint, and has been a source of ideas in the development of the device described in this paper.

We deduce that the electromagnetic signals measured in the tests performed so far have no representation in the usual context (see Fig. 6, right). One of the reasons is that the solutions of the 3D vector wave equation tend to be dispersive in a very short range (usually no more than one or two wavelengths), unless they display infinite energy [20]. In our experiments the distance from the antenna under test and the receiver allowed for 12 up to 60 wavelengths (depending on the signal frequency, whose range varied from 1 GHz to 5 GHz). Thus, the signal measured cannot belong to those modeled by the classical Maxwell's equations. This observation is important because the existence of the waves generated by our antennas is not trivially covered by standard theories. This motivates the study of suitable extensions of the electrodynamics equations. Many authors have devoted their efforts with the aim of detecting valuable alternatives. Existing literature is very rich. In this regard we just mention a few papers: [21], [22], [23], [24], [25], [26] [27],[28].

Since the pioneering paper [29] (see also [30]), modifications are usually obtained by proposing an alternative Lagrangian. Other possible justifications for the experiments described in this paper can be found in the material collected in [17] and [18] (see the appendices there for a quick review). There the Lagrangian is exactly the one of the usual Maxwell's equations, but the variations are subject to a further constraint that forces the solutions to follow the rules of geometrical optics. In this fashion one can build solutions as in (1) and (2), where the Poynting vector is perfectly lined up with the direction of motion. This property holds for plane waves of infinite extension, though is rarely found in the Maxwellian context (see for instance the case of spherical waves in the near-field regime [31]).

We just mention the version of that model that deals with the so called *free-waves*, being a complete discussion outside the scopes of the present paper. This reads as follows:

$$\frac{\partial \mathbf{E}}{\partial t} = c^2 \text{curl} \mathbf{B} - \mathbf{V} \text{div} \mathbf{E} \quad (5)$$

$$\frac{\partial \mathbf{B}}{\partial t} = - \text{curl} \mathbf{E} \quad (6)$$

$$\text{div} \mathbf{B} = 0 \quad (7)$$

$$(\mathbf{E} + \mathbf{V} \times \mathbf{B}) \text{div} \mathbf{E} = 0 \quad (8)$$

where \mathbf{V} is a suitable velocity field associated to the flow of energy of an electromagnetic wave. The system admits solutions where the vectors \mathbf{E} , \mathbf{B} , \mathbf{V} form orthogonal triplets. In this way, \mathbf{V} is lined up with the Poynting's vector given by $\mathbf{E} \times \mathbf{B}$. The expression in (1) is now solution by setting $\mathbf{V} = (0, 0, c)$, and for the one in (2) we have $\mathbf{V} = (c, 0, 0)$. In this context, the Gauss theorem still holds but should be interpreted in weak form by assuming that wells and

sources compensate along the path of a wave. This fact can be checked after a direct computation on the exact solutions. Of course, if $\text{div}\mathbf{E} = 0$, the field \mathbf{V} disappears and we return to the classical Maxwell's equations in vacuum. Note that the fields (1) and (2) solve a 1-D wave equation in the direction of propagation \mathbf{V} , though they occupy a volume in the transverse direction. Therefore, the great advantage of this approach is to be able to deal with a 1-D scalar wave equation in place of a 3-D vector one. According to P. Dirac, if we substitute f in (1) and (2) by a *delta* function, we are following the trajectory of a particle (photon) along an optical ray line. This passage has however no explicit mathematical justification, since such a distribution would not satisfy the whole set of eight Maxwell's equations in vacuum. It is instead compatible with the set of equations (5), (6), (7) and (8).

The last observations imply that the revised set of equation is perfectly compatible with the rules of geometrical optics. As a matter of fact, when \mathbf{V} is the gradient of a potential Ψ and its intensity is constantly equal to c , we obtain $|\mathbf{V}| = |\nabla\Psi| = c$, which is the stationary eikonal equation (see [29], section 3.1.4). Such a property is independent of the signal carried and describes the evolution of electromagnetic wave-fronts by optics. Moreover, the set of equations (5)-(8) derives from a Lagrangian, it is invariant under Lorenz transformations, and can be written in covariant form. This theoretical approach actually inspired the present research on antennas of a particular shape. The signals so generated confirm the predictions, also suggesting how the results can be possibly improved.

6 Further options and conclusions

We collected here a series of experiments aimed at showing that antennas of extremely high directivity can be actually built. The electromagnetic waves so produced have the property of preserving the topology of the magnetic field during the entire process that goes from the transmission of the signal inside the supplying coax cable up to the emission in open space. Our experiments actually confirm the existence of such waves. Conical type waves are similar to that shown in Fig. 2, bottom. We strongly believe that emission patterns exhibiting infinite directivity (Fig. 2, top) could be also generated with the help of the due technical effort. Indeed, we have all the elements to ameliorate the results obtained so far. The reader can easily realize that achieving perfect directivity would have a deep impact in many applications, in particular those requiring secure connections based on a high level of reliability (consider for instance banks, private companies, or military uses). In this way, RF data can be transferred between two stations through a beam that cannot be intercepted outside the segment joining the two parts.

The tests we made were based on two different strands. There are in fact experiments where the resonator is composed by opposite cones and the system of the two is embedded in a suitable dielectric lens. As we checked, performances are influenced by the shape of the dielectric medium. There are also documented

experiments where the dielectric is absent, and the resonators feature a peculiar shape (see Figs. 11, 12). Therefore, there is the possibility of combining these two approaches and play with “custom” antennae, where one can freely vary both the conductive part and the dielectric. The use of 3D printing techniques becomes then crucial.

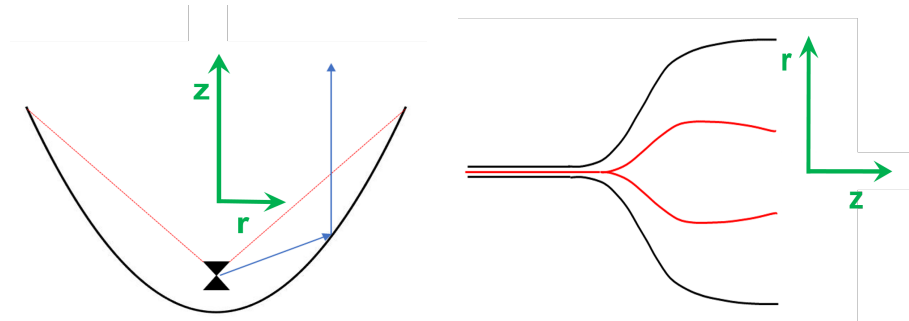


Figure 15: Left: A directive antenna where the biconical part lays at the focus of a large paraboloid. The displacement is rather different from the classical one, where the focus usually hosts a dipole whose orientation is not aimed at preserving the topology of the magnetic lines of force. Indeed, the break of these lines jeopardizes the directivity properties we are discussing in the present paper. Right: Possible design of an antenna where the signal from a coax passes through a resonating chamber before being definitively emitted. The 3D body of both antennas is obtained by rotating the pictures about the emission axis (z).

There is in addition a third pathway, which consists of exploring other reflector types. Here we used a conical reflector due to its simplicity of construction. Nevertheless, a parabolic type reflector could work as well (see Fig. 15, left). In this fashion, the biconic resonator must be put at the focus. The disadvantage is that the device becomes rather bulky. We could also take into account situations where the reflector is removed (see Fig. 15, right). Here the geometry becomes extremely decisive. The aim is always to preserve the circular topology of the lines of force of the magnetic field. The magnetic induction streamlines of the signal coming from the coax are closed transverse circles. These are somehow “dilated” when passing through the antenna device. If some conditions of resonance are met (strictly depending on shape and frequency), the wave could be expelled in open air. We have no idea however if such last experiment is feasible, though some preliminary tests have been already tried with little success.

We mention some negative effects that should be better investigated. One of them is the design of the area involved in the signal input. The gap between the cones must be as tiny as possible. In the geometries we tested here, the cones were too small to neglect this factor. This choice also forced us to work at higher frequencies, with the consequence of being more exposed to the various

imperfections of the prototypes. In addition, the solid printing of the dielectric in PLA, in the case of Type B, took many hours. Therefore, devices of larger size come at a nontrivial cost. When the input frequency is not high enough, the antenna does not resonate in the proper manner. The signal can escape from the edges at the base of the cones, generating unwanted effects. This could be an explanation of the appearance of secondary lobes at lower frequency (the spurious wave is directly radiated, without passing through the dielectric and the reflector). Such a fact is certainly true for the devices of Type C and D, where at certain angles the gap between the conductors is directly visible at naked eye, which implies that there are emitted rays that do not encounter the reflector. Notwithstanding the roughness of our first tests, we are proud to claim that the results are not bad at all.

Of course, we may elaborate more complicated situations were all the degrees of freedom (i.e., the shapes of the resonator, the dielectric and the reflector) are taken into consideration. These are the reasons why we are convinced that, one day, antenna devices displaying infinite directivity will become a reality. Point-to-point communications without dispersion can be then set up by using two antennas of the same kind both for transmission and reception.

References

- [1] Shukla M.K., Nguyen H.H., Pandey O.J (2020), Multiuser full-duplex IoT networks with wireless-powered relaying: Performance analysis and energy efficiency optimization, *IEEE Trans. Green Commun. Netw.*, **4**, 982–997.
- [2] Fantuzzi M. (2018), Design and Modelling of Wireless Power Transfer and Energy Harvesting Systems, Ph.D. Thesis, Alma Mater Studiorum Bologna.
- [3] Georgiou O., Wang S., Bocus M.Z., Dettmann C.P., Coon J.P. (2015), Directional antennas improve the link-connectivity of interference limited ad hoc networks, *Proc. IEEE 26th Annual Int. Symp. on Personal, Indoor, and Mobile Radio Comm. (PIMRC)*, Hong Kong, 1311–1316.
- [4] Pandey O.J., Gautam V., Nguyen H.H., Shukla M.K., Hegde R.M. (2020), Fault-Resilient Distributed Detection and Estimation Over a SW-WSN Using LCMV Beamforming, *IEEE Trans. Netw. Serv. Manag.*, **17**, 1758–1773.
- [5] Khalighi M.A., Uysal M. (2014), Survey on free space optical communication: A communication theory perspective, *IEEE Comm. Surv. Tutorials*, **16**, 2231–2258.
- [6] Ding T., Yi J., Li H., Zhang H., Burokur S.N. (2017), 3D field-shaping lens using all-dielectric gradient refractive index materials, *Nat. Sci. Rep.*, **7**, 782.

- [7] Dai H.N., Ng K.W., Li M., Wu M.Y. (2013), An overview of using directional antennas in wireless networks, *Int. J. Commun. Syst.*, **26**, 413–448.
- [8] Hurley C., Rogers R., Thornton F., Connelly D., Baker B. (2007) Chapter 2—Understanding Antennas and Antenna Theory. In *WarDriving and Wireless Penetration Testing*, Syngress: Rockland MA, 31–61.
- [9] Schelkunoff S.A. (1951), General theory of symmetric biconical antennas, *J. Applied Phys.*, **22**, 1330.
- [10] Tanaka H., Makino I., Shimano H., Muramatsu H. (2016), An evaluation of using small biconical antennas in normalized site attenuation measurements, *IEEE Int. Symp. on Electromagnetic Compatibility (EMC)*, Ottawa.
- [11] Black D., Brunasso T. A. (2006), An ultra-wideband bicone antenna, *IEEE Int. Conf. on Ultra-Wideband*.
- [12] Remez J., Ben-Ari E. (2009) Low-loss wideband multimodal interferometric antenna for DOA in azimuth and elevation, *IEEE Antennas and Wireless Propagation Letters*, **8**, 898 - 902.
- [13] Ghalibafan J., Hashemi S. M. (2018), Design of an asymmetric capped biconical antenna for constant beam direction over a desired range of frequencies, *AEU - Int. J. Electronics and Communications*, **84**, 27-33.
- [14] Shi L., Sun H.-J., Dong W.-W., Lv X. (2009), A dual-band multifunction carborne hybrid antenna for satellite communication relay system, *Progress In Electromagnetics Research*, **95**, 329-340.
- [15] Vacchione J. et al. (2012), Telecommunications antennas for the Juno mission to Jupiter, *IEEE Aerospace Conference Proceedings*.
- [16] Chiolerio A., Diazz L., Funaro D. (2020), Highly directive biconic antennas embedded in a dielectric, *Appl. Sci.*, MDPI, **10**, 24, 8828.
- [17] Funaro, D. (2008), *Electromagnetism and the Structure of Matter*; World Scientific: Singapore.
- [18] Funaro, D. (2019) *From Photons to Atoms, The Electromagnetic Nature of Matter*; World Scientific: Singapore.
- [19] Huber E. et al. (2016), Dielectric property measurement of PLA, *IEEE Int. Conf. on Electro Information Technology (EIT)*.
- [20] Sezginer A. (1985), A general formulation of focus wave modes, *J. Appl. Phys.*, **57**, pp. 678–683.
- [21] Arbab I. (2017), Extended electrodynamics and its consequences, *Mod. Phys. Lett. B*, **31**, 9, 1750099.

- [22] Benci V., Fortunato V. (2004), Towards a unified field theory for classical electrodynamics, *Arch. Rat. Mech. Anal.*, **173**, pp. 379–414.
- [23] Coclite G. M., Georgiev V. (2004), Solitary waves for Maxwell Schrödinger equations, *Electronic J. Differ. Eq.*, **94**, pp. 1–31.
- [24] Donev S., Tashkova M. (2014), *Geometric view on photon-like objects*, LAP LAMBERT Academic Publishing.
- [25] Harmuth H. F., Barrett T. W., Meffert B. (2001), *Modified Maxwell Equations in Quantum Electrodynamics*, SCCP, Vol. 19, World Scientific.
- [26] Hively L. M., Giakos G. C.. (2012), Toward a more complete electrodynamic theory, *IJSISE*, **5**, 1, pp. 3–10.
- [27] Lehnert B., Roy S. (1998), *Extended Electromagnetic Theory: Space Charge in Vacuo and the Rest Mass of the Photon*, SCCP, Vol. 16, World Scientific.
- [28] Munz C.-D., Schneider R., Sonnendrücker E., Voss U. (1999), Maxwell's equations when the charge conservation is not satisfied, *C. R. Acad. Sci. Paris*, **328**, Série I, pp. 431–436.
- [29] Born M., Infeld L. (1934), Foundations of the new field theory, *Proc. R. Soc. Lon. A*, **144**, pp. 425–451.
- [30] Yang Y. (2000), Classical solutions in the Born-Infeld theory, *Proc. R. Soc. Lon. A*, **456**, pp. 615–640.
- [31] Jackson J. D. (2006), How an antenna launches its input power into radiation: The pattern of the Poynting vector at and near an antenna, *American Journal of Physics* 74, p. 280.
- [32] Born M., Wolf E. (1987), *Principles of Optics*, Pergamon Press, Oxford.